

Holographic optical trapping

David G. Grier and Yael Roichman

*Department of Physics and Center for Soft Matter Research,
New York University, 4 Washington Place, New York, NY 10003*

Holographic optical tweezers use computer-generated holograms to create arbitrary three-dimensional configurations of single-beam optical traps useful for capturing, moving and transforming mesoscopic objects. Through a combination of beam-splitting, mode forming, and adaptive wavefront correction, holographic traps can exert precisely specified and characterized forces and torques on objects ranging in size from a few nanometers to hundreds of micrometers. With nanometer-scale spatial resolution and real-time reconfigurability, holographic optical traps offer extraordinary access to the microscopic world and already have found applications in fundamental research and industrial applications.

Key words: Optical trapping, computational holography, digital video microscopy

I. INTRODUCTION

Two decades after their invention, single-beam optical gradient force traps, commonly known as optical tweezers, have become indispensable tools for research [1, 2]. Formed by bringing an intense beam of light to a diffraction-limited focus, an optical tweezer can capture an object ranging in size from a few nanometers to several micrometers and hold it stably in three dimensions against gravity, random thermal forces, and other external influences. This article addresses a generalization of the optical tweezer technique that uses computer-generated holograms (CGH) to create hundreds of simultaneous optical tweezers in arbitrary three-dimensional configurations, each with individually specified trapping characteristics. Introduced in 1997, holographic optical traps [3, 4, 5, 6, 7, 8] have found applications in research and engineering ranging from fundamental studies of the mechanisms of phase transitions to the manufacture of wavelength-scale devices [9].

A single optical tweezer works by minimizing the electromagnetic energy stored in the fields scattered and absorbed by an illuminated object [10]. Generally, this results in a small object being localized near the focus of a strongly converging laser beam. Heuristically, and semi-quantitatively for sub-wavelength-scale Rayleigh objects, the attractive force may be understood as arising from a dipole moment induced in the particle by the light's fields. The induced dipole is drawn up gradients of the field toward the focus, where the light is brightest. Because the induced dipole moment typically is proportional to the field and the force on the dipole is proportional to the local field gradient, the overall trapping force is proportional to gradients in the intensity. This insight is exploited in the next section to simplify the creation of holographic trapping arrays.

Radiation pressure due to absorption and backscattering competes with the attractive gradient force and tends to blow particles downstream. Stable three-dimensional trapping in a single beam of light is possible only if the axial intensity gradients are large enough to overcome radiation pressure. This is one reason that optical twee-

zers generally are created with high-numerical-aperture lenses, such as microscope objectives, that are capable of bringing a beam of light to an exceptionally tight focus. Geometric aberrations degrade an optical tweezer's performance by reducing the focal spot's intensity gradients. Microscope objectives' well corrected aberrations also recommend them for this application.

A single collimated beam that fills an infinity-corrected objective's input pupil comes to a focus and forms a trap in the lens' focal plane at a position dictated by the beam's angle of incidence. Any object trapped in the tweezer therefore can be imaged conveniently with the same lens, provided that the imaging illumination can be separated from the trap-forming laser, for instance with a dichroic mirror. A diverging beam filling the lens' input pupil forms a trap downstream of the focal plane, and a converging beam forms a trap upstream. Controlling the input beam's degree of collimation and angle of incidence therefore provides a mechanism for positioning an optical tweezer in three dimensions.

II. HOLOGRAPHIC OPTICAL TRAPPING

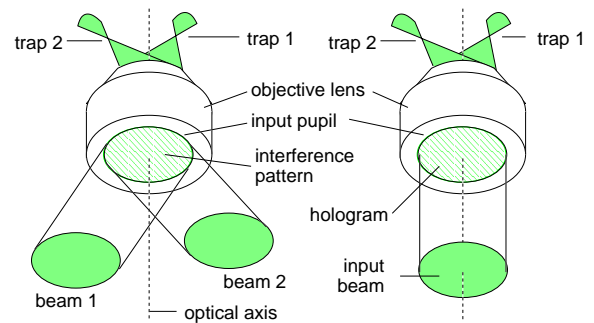


FIG. 1: Two beams of light focus to two optical tweezers, and also form an interference pattern at the lens' input pupil. The same traps can be created from a single input beam by placing an equivalent hologram in the input pupil.

Multiple beams of light all passing through the ob-

jective's input pupil with their own angle of incidence and degree of collimation create a configuration of optical traps, as shown in Fig. 1. If these beams are mutually coherent, they form an interference pattern in the input pupil, with fields of the form

$$\psi(\boldsymbol{\rho}) = u(\boldsymbol{\rho}) \exp(-i\varphi(\boldsymbol{\rho})), \quad (1)$$

at point $\boldsymbol{\rho}$. Were the same pattern of amplitude modulations, $u(\boldsymbol{\rho})$, and phase modulations, $\varphi(\boldsymbol{\rho})$, imposed on the wavefronts of a single incident beam as it passed through the input pupil, the modified beam also would create the same trapping pattern. This is the principle behind holographic optical trapping.

Creating multiple optical traps does not require a fully complex hologram. Because optical trapping relies only on gradients in the intensity, and not on the phase, even quite complicated three-dimensional configurations of optical traps can be specified with just $\varphi(\boldsymbol{\rho})$, leaving the amplitude profile $u(\boldsymbol{\rho}) = u_0(\boldsymbol{\rho})$ of the input beam unchanged. The phase-only diffractive optical element (DOE) encoding a particular pattern of traps is an example of a class of holograms known as kinoforms. The trick, then, is to compute the kinoform that projects a particular pattern of traps.

Several algorithms have been proposed for seeking holograms that most accurately and most rapidly approximate desired trapping patterns. The fastest is to compute the phase associated with a linear superposition of the desired beams, and to simply discard the associated amplitude variations [5]. Such straightforward superposition is surprisingly effective, particularly if the beams are chosen to have random relative phases. The resulting trapping pattern tends to be marred, however, by large numbers of "ghost" traps at symmetry-dictated positions, and also by large variations in the traps' intensities from their design values. For many applications, however, the resulting performance is more than adequate, and the ease of computation facilitates real-time interactive control.

Superposition also provides an outstanding starting point for refinement algorithms. Iterative refinement schemes based on the Gerchberg-Saxton and adaptive additive algorithms [11] improve all aspects of the holograms' performance [6, 12], although at substantial computational cost, particularly for three-dimensional trapping patterns. A modified adaptive-additive algorithm that calculates fields only at the traps' locations [7] is far more efficient, but also less effective at suppressing ghost traps. More recently, direct search algorithms have been shown to yield substantially more accurate DOE estimates [8] and also can be far more efficient if started from the randomly-phased superposition [8] rather than from a random phase field [12].

The field due to an array of M discrete point-like traps

located at $\{\mathbf{r}_m\}$ can be approximated by

$$\psi(\mathbf{r}) = \sum_{m=1}^M \psi_m \delta(\mathbf{r} - \mathbf{r}_m), \quad \text{with} \quad (2)$$

$$\psi_m = \alpha_m \exp(-i\phi_m), \quad (3)$$

where α_m is the relative amplitude of the m -th trap, normalized by $\sum_{m=1}^M |\alpha_m|^2 = 1$. The relative phases, ϕ_m , generally are assigned randomly, but also may be specified for particular applications. In most practical implementations, such as that depicted in Fig. 2, the DOE, $\varphi(\boldsymbol{\rho})$, encoding the traps also is discretized into an array of N phase pixels φ_j located at $\boldsymbol{\rho}_j$. Consequently, the complex field at each trap can be described by a nonlinear transformation of the input phase

$$\psi_m = \sum_{j=1}^N T_{m,j} u_j \exp(i\varphi_j), \quad (4)$$

where the transfer matrix $T_{m,j}$ describes the coherent propagation of light from pixel j on the DOE to trap m in the focal plane, given the input beam's amplitude profile, $u_j = u_0(\boldsymbol{\rho}_j)$. In our implementation, the amplitude profile is approximated by the Heaviside step function $u_0(\boldsymbol{\rho}) = \Theta(\rho - R)$, where R is the radius of the optical train's aperture.

The transfer matrix for a two-dimensional configuration of conventional optical tweezers is given in scalar diffraction theory by [8, 13]

$$T_{m,j}^{(0)} = \frac{1}{\lambda f} \exp\left(-i \frac{2\pi \mathbf{r}_m \cdot \boldsymbol{\rho}_j}{\lambda f}\right). \quad (5)$$

More generally, the transfer matrix can take the form

$$T_{m,j} = \prod_{k=0}^{K_m} T_{m,j}^{(k)}, \quad (6)$$

where the additional K_m contributions, $T_{m,j}^{(k)}$, describe wavefront-shaping operations specific to the m -th trap. For example, if the DOE displaces the m -th trap by a distance z_m along the optical axis, then

$$T_{m,j}^z = \exp\left(i \frac{2\pi \rho_j^2 z_m}{f^2}\right) \quad (7)$$

returns its image to the focal plane for analysis [7, 8]. More dramatic transformations implemented with Eq. (6) will be described in Sec. V.

Direct search refinement starts from an estimate φ_j for the DOE, and the associated fields ψ_m calculated with Eq. (4). If the DOE exactly encoded the desired trapping pattern, then the calculated amplitudes $|\psi_m|$ would agree with the design values, α_m . The algorithm seeks to minimize actual discrepancies between $|\psi_m|$ and α_m .

Following Meister and Winfield [14], we adopt the error function

$$E = -\langle |\psi_m|^2 \rangle + \gamma \sqrt{\left\langle \left(|\psi_m|^2 - \alpha_m^2 \frac{\langle |\psi_m|^2 \alpha_m^2 \rangle}{\langle \alpha_m^4 \rangle} \right)^2 \right\rangle}, \quad (8)$$

where the weighting factor γ sets the relative importance attached to diffraction efficiency ($\gamma = 0$) and fidelity to design ($\gamma > 0$). Improvements are sought by selecting pixels at random, changing their phase values, recomputing the fields, and retaining only those proposed changes that improve the performance. Because the relationship between $|\psi_m|$ and φ_j is inherently nonlinear, the search proceeds sequentially, and the process continues until E is reduced to an acceptable level.

In practice, convergence starting from a randomly-phased superposition typically is achieved with a single pass through the array, for a total of MN operations. This is comparable in computational cost to the initial superposition and so roughly doubles the total cost of the computation. The benefits of the refinement step can be substantial, as a practical example illustrates.

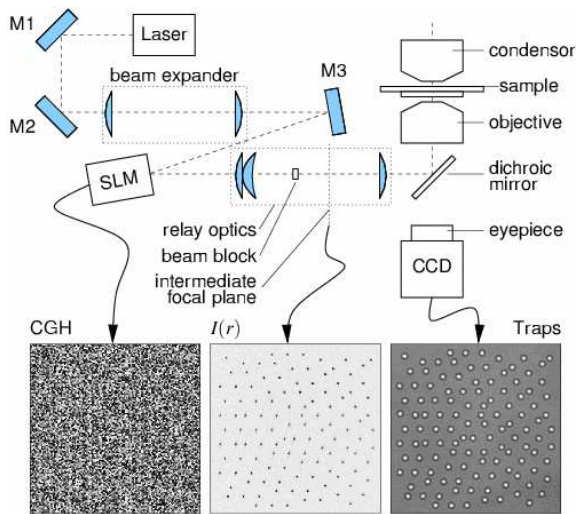


FIG. 2: Schematic implementation of holographic optical traps. An expanded laser beam is reflected by a liquid crystal spatial light modulation, which imprints a computer-generated hologram onto its wavefronts. The 200×200 pixel region of a CGH shown encodes a pattern of 119 optical tweezers in a quasiperiodic arrangement. The phase hologram is relayed to the input pupil of an objective lens that focuses it into holographic optical traps, shown here trapping $1.5 \mu\text{m}$ diameter colloidal spheres in water.

We project holographic optical traps with the system shown schematically in Fig. 2. Light from a frequency-doubled Nd:YVO₄ laser (Coherent Verdi) is expanded to fill the face of a reflective liquid crystal spatial light modulator (SLM) (Hamamatsu X8267-16 PPM), which can impose a phase shift between 0 and 2π radians at each pixel in a 768×768 array. The phase-modified beam is

relayed to the input pupil of a $100\times$, NA 1.4, SPlan Apo oil immersion objective mounted in a Nikon TE-2000U inverted optical microscope, which focuses the light into optical traps. Because the SLM's face is in a plane conjugate to the objective's input pupil, the effect is the same as if the DOE were placed in the input pupil, as in Fig. 1. The benefit of this arrangement is that the trapped sample can be imaged onto a CCD camera using the microscope's standard optical train, with the imaging illumination passing through the dichroic mirror used to direct the trap-forming laser.

In practice, not all of the input beam is diffracted by the SLM, and the undiffracted portion ordinarily would form a bright trap right in the middle of the field of view. To counter this, we adjust the beam expander so that the SLM is illuminated with a slightly converging beam. Projecting optical traps into the microscope's focal plane therefore requires the traps to be displaced along the optical axis with the computed DOE. The undiffracted beam therefore focuses into a different plane within the relay optics than the intended traps, and so can be blocked with a spatial filter without disrupting the traps. Displacing the trapping plane has the additional benefit of projecting most residual ghost traps out of the sample volume.

The result can be seen in the typical images in Fig. 2. Here, an eight-bit CGH imprinted on the input beam by the SLM creates the pattern of focal spots in the intermediate focal plane, which is shown trapping colloidal spheres dispersed in water. This particular quasiperiodic arrangement of 119 optical traps is particularly challenging because it lacks reflection symmetry about the optical axis. As a result, a typical DOE computed by superposition alone suffers from more than 50 percent root-mean-squared (RMS) relative deviations from design amplitudes. Imaging photometry and measurements of the traps' potential energy wells by particle tracking [8, 15] confirm that the DOE refined by direct search is uniform to within 5 percent, a factor of ten improvement.

Our implementation of dynamic holographic optical trapping permits full three-dimensional manipulation over a $100 \times 100 \times 40 \mu\text{m}^3$ volume. Micrometer-scale colloidal spheres are readily stacked five or more deep along the axial direction, with three-dimensional quasicrystals consisting of hundreds of spheres having recently been demonstrated [16]. The arrays' fidelity to design intensities, and the DOE's overall efficiency fall off as the arrays become increasingly complicated. How design complexity affects implementational efficacy has yet to be worked out.

Demonstrations of three-dimensional control [5, 12] such as the rotating icosahedron in Fig. 3, reveal that objects can be organized into vertical stacks along the optical axis. Three-dimensional assemblies consisting of hundreds of spheres in asymmetric configurations up to nine layers deep recently have been demonstrated [16]. Still larger areas and depths can be accessed, at least in principle, by creating time-shared three-dimensional

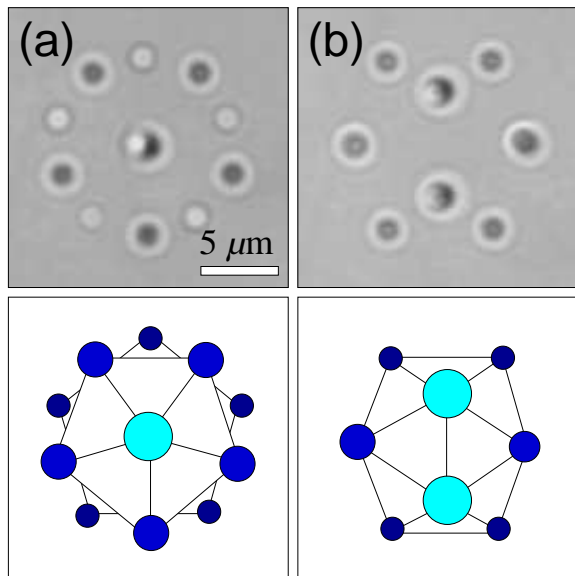


FIG. 3: Two views of a rotating icosahedron of colloidal spheres created with dynamic holographic optical tweezers.

trapping patterns [17]. The resulting structures can be made permanent, for example by gelling the suspending fluid [18, 19].

III. STATIC OPTICAL LANDSCAPES: TRANSPORT AND FRACTIONATION

Dynamic optical trapping arrays have immediate applications for manipulating microscopic objects such as biological cells and organizing them into useful and interesting configurations. The speed with which patterns consisting of hundreds of simultaneous traps can be animated with conventional computing hardware lends itself to interactive real-time manipulation, as indeed is the case for the commercial implementation of this technology (BioRyx 200 system, Arrayx, Inc.). Even static optical trapping arrays, however, have surprising and practical applications.

Each optical trap in an array acts as a three-dimensional potential energy well for a small object. An entire array, therefore, may be viewed as an extended potential energy landscape whose symmetries and features can be programmed precisely. Static optical landscapes are useful for templating the crystallization of uniformly sized colloidal particles, and more generally in modifying such dispersions' phase transitions and dynamics [20, 21]. How individual colloidal particles navigate such landscapes when driven by an external force has proved a surprisingly challenging problem with immediate technological applications.

Figure 4 shows the measured [15, 22] trajectories of colloidal spheres as they are carried by flowing water through a 10×10 square array of holographic optical

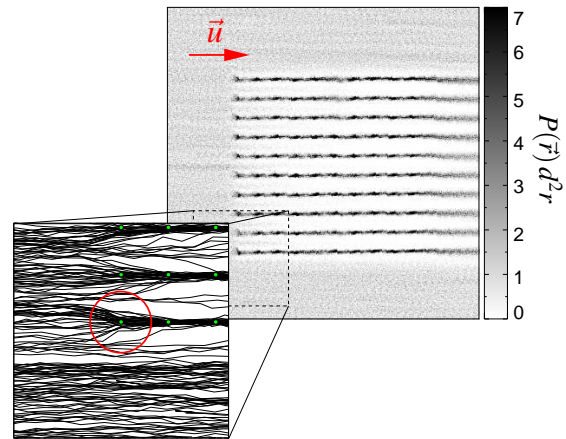


FIG. 4: Measured trajectories of fluid-borne micrometer-diameter colloidal particles encountering a 10×10 square array of holographic optical traps with a lattice constant of $3 \mu\text{m}$.

traps. At flow speeds of $u = 50 \mu\text{m}/\text{sec}$, the force due to viscous drag on the $\sigma = 1.5 \mu\text{m}$ diameter silica spheres is comparable to the individual tweezers' maximum trapping force. Although particles are drawn toward the rows of tweezers from a range comparable to their diameter, they hop freely from trap to trap along the array's [10] axis. The particles' channeling along the rows is clearly demonstrated by the compiled probability density $P(\mathbf{r}) d\mathbf{r}$ for finding particles within $d\mathbf{r}$ of \mathbf{r} relative to the bulk, which also is plotted in Fig. 4.

Tilting the array so that its [10] axis no longer is aligned with the flow presents the particles with an opportunity to escape from their commensurate paths through the potential energy landscape. Over some range of angles, however, a particle can be deflected enough by its encounter with one trap to fall into the domain of attraction of the next. In this case, the particle's trajectory can remain kinetically locked in to the commensurate direction through the landscape [22].

Fluid-borne objects can become kinetically locked-in to even a single inclined line of traps [23, 24], as the data in Fig. 5 show. This effect has immediate technological implications. Because the potential energy landscape experienced by a passing particle depends sensitively on the object's optical form factor [24], small differences in size, shape or composition can cause different objects to follow radically different paths through an optical trap array. The resulting spatial separation is the basis for a continuous and continuously tunable sorting process known as optical fractionation [23, 25].

Although the theory for transport through optical tweezer arrays is not yet complete [24, 26], preliminary results suggest that optical fractionation may be able to sort flowing objects with exponential size selectivity [23, 24]. Two-dimensional and three-dimensional arrays, moreover, exhibit a rich hierarchy of kinetically locked-in commensurate pathways [22, 26], all of which can be

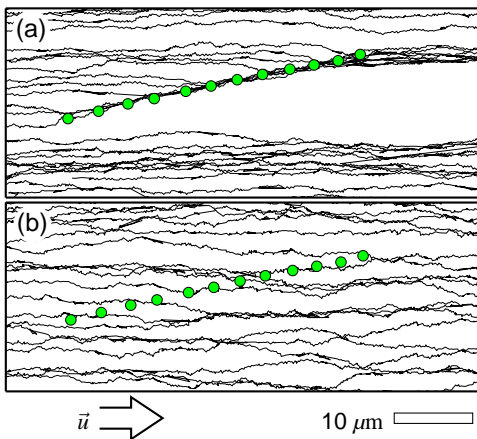


FIG. 5: Optical fractionation. (a) Measured trajectories of large colloidal spheres, $1.58 \mu\text{m}$ in diameter, dispersed in water flowing at $50 \mu\text{m}/\text{sec}$, are deflected by a line of 12 holographic optical traps, whose positions are indicated by circles. (b) Smaller $1 \mu\text{m}$ diameter spheres dispersed in the same flow are not deflected (b).

exploited for multi-channel sorting.

The first generation of experiments [22, 23, 25] has relied on driving forces exerted by flowing fluid. Symmetry-guided transport also should arise for particles driven by electrophoresis, electroosmosis and related mechanisms. Field-driven optical fractionation will make possible sorting on the basis of such properties as surface charge density and should be useful for processes monitoring and control and could provide the basis for a new family of analytical chromatographies.

IV. ACTIVE LANDSCAPES: CONVEYORS AND RATCHETS

While static optical trap arrays act as filters or prisms for externally driven dispersions, dynamic arrays are useful for inducing motion. Dynamic holographic optical traps do not move continuously, as do optical tweezers scanned with moving mirrors [27] or traps created by the generalized phase contrast method [28]. Rather, one pattern of traps dissolves into another as the DOE encoding the first is replaced by that encoding the second. If trapped objects diffuse slowly enough, they still can be passed from trap to trap by rapidly updating the phase hologram. Viscous relaxation, in this case, plays the role in active holographic transport that persistence of vision plays in cartoon animation to provide the appearance of continuous motion.

Sequences of overlapping trapping patterns can dynamically organize mesoscopic objects into arbitrary three-dimensional configurations, and reorganize them quasi-continuously [4, 5, 7, 12, 16, 19, 29]. Periodically cycled sequences of as few as three holograms can induce complicated patterns of motion over large areas through

a process called optical peristalsis [30]. Here, an object is transferred forward from one manifold of traps in a given pattern to the next by two or more intervening trapping patterns whose manifolds bridge the gap. The sequence of patterns breaks spatiotemporal symmetry and ensures that motion proceeds in the intended direction. Unlike interactive manipulation that requires an individual particle to be captured and its path to be calculated, optical peristalsis operates over the entire field of view, directing and orienting objects automatically through small sequences of precalculated holograms, much like an optical conveyor belt.

This process also provides a means to implement a so-called thermal ratchet [31], in which diffusing particles' random Brownian motion is rectified into a directed flux by a time-evolving potential energy landscape. Unlike conventional motors and deterministic processes such as optical peristalsis whose performance is degraded by random fluctuations, thermal ratchets are stochastic machines and *require* noise to operate. Most proposed models for thermal ratchets exploit a space-filling spatially asymmetric potential energy landscape. Breaking spatial symmetry is not enough to eke a flux out of fluctuations for a system in equilibrium. As part of a sequence of states driving the system out of equilibrium, however, it can help to break diffusion's spatiotemporal symmetry and thereby induce motion. This works even if the landscape itself has no overall slope and thus exerts no net force.

A regular array of holographic optical tweezers, such as that shown in Fig. 6, presents a potential energy landscape that neither fills space nor breaks spatial symmetry. Even the individual traps are locally symmetric potential wells. Nevertheless, translating the array first by one third of a lattice constant, then by two, and then returning it to its initial state creates a discrete-state traveling ratchet [32] whose time evolution breaks spatiotemporal symmetry. The resulting motion differs from that induced by optical peristalsis in a way that leads to additional applications.

If the lattice constant L is comparable to the traps' effective widths [24], then the traveling ratchet reduces to an example optical peristalsis, and particles are deterministically translated along the displacement direction. Increasing the separation causes particles trapped in one state to be left behind in a flat and featureless region of the potential energy landscape in the next state. They must diffuse to the nearest manifold of traps before they can be localized and transported. If the time τ required for the particles to diffuse across the potential energy plateau is shorter than the duration T of each state, then most particles are transported forward. On the other hand, if the particles diffuse too slowly, they can miss the forward-going wave and may end up instead being transported *backward* [32]. Such flux reversal as a function of cycle time T and trap separation L is a hallmark of thermal ratchet operation, and is clearly seen in the data in Fig. 6.

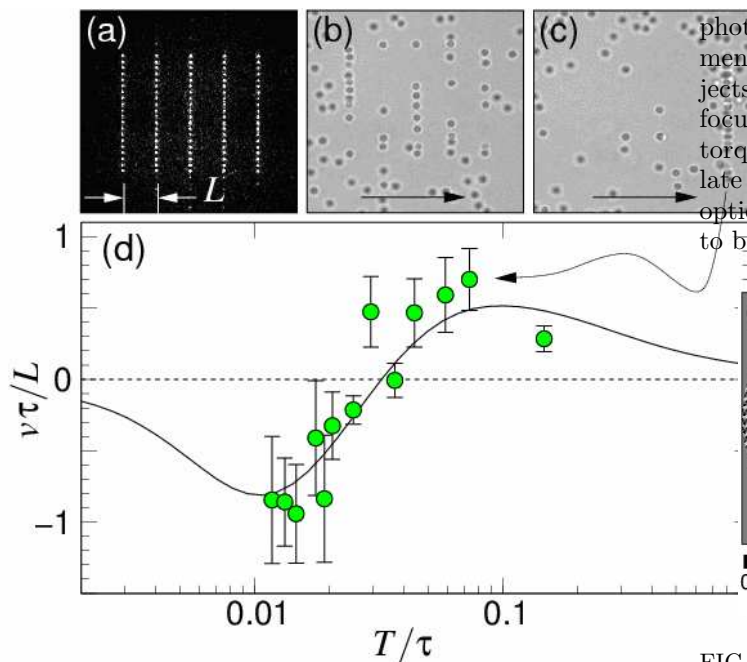


FIG. 6: A thermal ratchet implemented with holographic optical tweezers. (a) The focused light from a 20×5 array with manifolds separated by $L = 3.8 \mu\text{m}$. (b) A dispersion of $1.58 \mu\text{m}$ diameter spheres interacting with the array. (c) After repeated displacements of the array by $L/3$ and $2L/3$, with each step lasting $T = 5$ sec, all the spheres are translated to the right. (d) The transport velocity v as a function of dwell time shows flux reversal as the cycle rate increases.

Flux reversal in microfabricated thermal ratchets already has been exploited for separating DNA and other macromolecules on the basis of their diffusivity [33]. The holographically implemented variant complements optical fractionation by permitting automatic sorting *in situ*. Variants of the holographic optical ratchet exploit more subtle symmetries to achieve simpler operation [34] or more sophisticated configurations of tweezers to optimize sorting.

V. MULTIMODE TRAPS

The previous sections addressed some of the applications for holographic arrays of conventional optical tweezers. Wavefront engineering through Eq. (6) provides access to more sophisticated traps. For example, the deceptively simple phase profile, $\varphi_\ell(\mathbf{r}) = \ell\theta$, where θ is the azimuthal angle around the optical axis and ℓ is an integer winding number, transforms a conventional TEM₀₀ mode into a helical mode [35]. The axial screw dislocation introduced by this phase profile leads to perfect destructive interference along the beam's axis. A helical beam consequently focuses to a *dark spot*, its intensity being redistributed into an annulus whose radius [36, 37, 38] scales with the topological charge ℓ . Each

photon in a helical mode carries $\ell\hbar$ orbital angular momentum [35, 39] that it can transfer to illuminated objects [40]. The ring-like optical trap that results from focusing a helical mode [41, 42, 43] therefore can exert torques on trapped objects [40], causing them to circulate around the ring [37, 44, 45]. Such torque-exerting optical traps, and their generalizations [46], have come to be known as optical vortices.

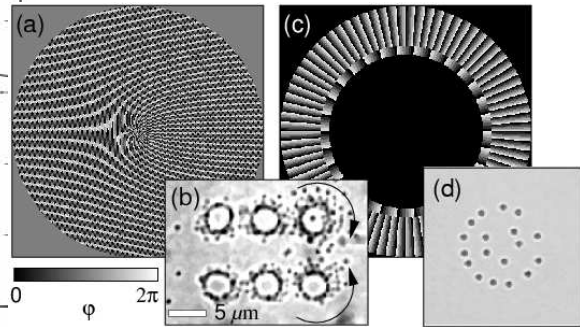


FIG. 7: (a) Phase mask encoding a 3×2 array of counter-rotating optical vortices with $\ell = \pm 30$. (b) Microoptomechanical pump created by projecting the vortex array into a colloidal dispersion. Fluid flows from right to left as the rings of particles circulate. (c) Phase mask encoding concentric optimized optical vortices. (d) A microoptomechanical Couette rheometer created by projecting the concentric vortices into a colloidal dispersion.

The vortex-forming phase profile can be imposed on an individual trap in an array in much the same way as the displacement-inducing curvature described by Eq. (7). As a result, a single DOE such as the example in Fig. 7(a) can create arrays of optical vortices, each with independently specified positions, intensities, and topological charges. Figure 7(b) shows the array of $\ell = +30$ and $\ell = -30$ optical vortices encoded by this DOE trapping and 700 nm diameter silica spheres. The rapidly circulating spheres entrain flows in the suspending water, which results in a steady stream along the axis of the array [47].

Unlike conventional trap-forming holograms, the helical phase profile $\varphi_\ell(\mathbf{r})$ has a topological defect at the origin. Regions of the DOE nearest the singularity contribute to an optical vortex's intensity at its outer edge, while more removed regions contribute to its inner edge [48]. This bright inner edge, moreover, is where an optical vortex traps and circulates particles. Removing the central region of a helical mode-former, as in Fig. 7(c) does not affect the optical vortex's performance as a torque-exerting optical trap, but reduces the amount of wasted light. The empty central region then can play host to one or more additional optical vortices [48, 49], as shown in Fig. 7(d). These concentric rings act as a microscopic Couette rheometer useful for studying viscoelastic properties at the nanometer to micrometer scale [49].

More general superpositions of helical modes give rise to other microoptomechanical devices, such as optical cogwheels [50] that are useful for sorting objects by size,

modulated optical vortices [46] that project objects on complicated trajectories through the focal plane.

A conical phase profile transforms an optical tweezer into a diffractionless Bessel beam [51, 52] that can stack objects into three dimensional columns. Adding helical and conical profiles creates generalized Bessel-Laguerre traps that also exert both torques and forces over extraordinarily larger ranges. Combining them by multiplication generates spiral intensity patterns whose trapping applications have yet to be fully investigated [53].

It should be emphasized that all of the microscopic manipulations described in this article, and a great many

more, can be accomplished with a single optical train. Strikingly different functionalities result from changes in the transfer matrices in Eq. (4), all under software control. Some already have provided new avenues for fundamental research. Others are making inroads into industrial processes. In the broadest sense, holographic optical trapping provides a powerful and very general approach to interacting with the microscopic world. Progress in both the technique and its real-world applications should be rapid.

This work was supported by NSF Grants number DBI-0233971 and DMR-0451589.

-
- [1] A. Ashkin, J. M. Dziedzic, J. E. Bjorkholm, and S. Chu, "Observation of a single-beam gradient force optical trap for dielectric particles," *Opt. Lett.* **11**, 288–290 (1986).
- [2] A. Ashkin, "History of optical trapping and manipulation of small-neutral particle, atoms, and molecules," *IEEE J. Sel. Top. Quantum Elec.* **6**, 841–856 (2000).
- [3] E. R. Dufresne and D. G. Grier, "Optical tweezer arrays and optical substrates created with diffractive optical elements," *Rev. Sci. Instr.* **69**, 1974–1977 (1998).
- [4] M. Reicherter, T. Haist, E. U. Wagemann, and H. J. Tiziani, "Optical particle trapping with computer-generated holograms written on a liquid-crystal display," *Opt. Lett.* **24**, 608–610 (1999).
- [5] J. Liesener, M. Reicherter, T. Haist, and H. J. Tiziani, "Multi-functional optical tweezers using computer-generated holograms," *Opt. Comm.* **185**, 77–82 (2000).
- [6] E. R. Dufresne, G. C. Spalding, M. T. Dearing, S. A. Sheets, and D. G. Grier, "Computer-generated holographic optical tweezer arrays," *Rev. Sci. Instr.* **72**, 1810–1816 (2001).
- [7] J. E. Curtis, B. A. Koss, and D. G. Grier, "Dynamic holographic optical tweezers," *Opt. Comm.* **207**, 169–175 (2002).
- [8] M. Polin, K. Ladavac, S.-H. Lee, Y. Roichman, and D. G. Grier, "Optimized holographic optical traps," *Opt. Express*, submitted for publication (2005).
- [9] D. G. Grier, "A revolution in optical manipulation," *Nature* **424**, 810–816 (2003).
- [10] P. A. Maia Neto and H. M. Nussenzveig, "Theory of optical tweezers," *Europhys. Lett.* **50**, 702–708 (2000).
- [11] V. Soifer, V. Kotlyar, and L. Doskolovich, *Iterative Methods for Diffractive Optical Elements Computation* (Taylor & Francis, Bristol, PA, 1997).
- [12] G. Sinclair, P. Jordan, J. Courtial, M. Padgett, J. Cooper, and Z. J. Laczik, "Assembly of 3-dimensional structures using programmable holographic optical tweezers," *Opt. Express* **12**, 5475–5480 (2004).
- [13] J. W. Goodman, *Introduction to Fourier Optics*, 2nd ed. (McGraw-Hill, New York, 1996).
- [14] M. Meister and R. J. Winfield, "Novel approaches to direct search algorithms for the design of diffractive optical elements," *Opt. Comm.* **203**, 39–49 (2002).
- [15] J. C. Crocker and D. G. Grier, "Methods of digital video microscopy for colloidal studies," *J. Colloid Interface Sci.* **179**, 298–310 (1996).
- [16] Y. Roichman and D. G. Grier, "Assembly of colloidal quasicrystals with holographic optical tweezers," *Opt. Express*, submitted for publication (2005).
- [17] H. Melville, G. F. Milne, G. C. Spalding, W. Sibbett, K. Dholakia, and D. McGloin, "Optical trapping of three-dimensional structures using dynamic holographic optical tweezers," *Opt. Express* **11**, 3562–3567 (2003).
- [18] P. T. Korda, G. C. Spalding, E. R. Dufresne, and D. G. Grier, "Nanofabrication with holographic optical tweezers," *Rev. Sci. Instr.* **73**, 1956–1957 (2002).
- [19] P. Jordan, H. Clare, L. Flendrig, J. Leach, J. Cooper, and M. Padgett, "Permanent 3D microstructures in a polymeric host creating using holographic optical tweezers," *J. Mod. Opt.* **51**, 627–632 (2004).
- [20] P. T. Korda, G. C. Spalding, and D. G. Grier, "Evolution of a colloidal critical state in an optical pinning potential," *Phys. Rev. B* **66**, 024504 (2002).
- [21] K. Mangold, P. Leiderer, and C. Bechinger, "Phase transitions of colloidal monolayers in periodic pinning arrays," *Phys. Rev. Lett.* **90**, 158302 (2003).
- [22] P. T. Korda, M. B. Taylor, and D. G. Grier, "Kinetically locked-in colloidal transport in an array of optical tweezers," *Phys. Rev. Lett.* **89**, 128301 (2002).
- [23] K. Ladavac, K. Kasza, and D. G. Grier, "Sorting by periodic potential energy landscapes: Optical fractionation," *Phys. Rev. E* **70**, 010901(R) (2004).
- [24] M. Pelton, K. Ladavac, and D. G. Grier, "Transport and fractionation in periodic potential-energy landscapes," *Phys. Rev. E* **70**, 031108 (2004).
- [25] M. P. MacDonald, G. C. Spalding, and K. Dholakia, "Microfluidic sorting in an optical lattice," *Nature* **426**, 421–424 (2003).
- [26] A. Gopinathan and D. G. Grier, "Statistically locked-in transport in periodic potential landscapes," *Phys. Rev. Lett.* **92**, 130602 (2004).
- [27] K. Sasaki, M. Koshio, H. Misawa, N. Kitamura, and H. Masuhara, "Pattern formation and flow control of fine particles by laser-scanning micromanipulation," *Opt. Lett.* **16**, 1463–1465 (1991).
- [28] P. C. Mogensen and J. Glückstad, "Dynamic array generation and pattern formation for optical tweezers," *Opt. Comm.* **175**, 75–81 (2000).
- [29] J. Leach, G. Sinclair, P. Jordan, J. Courtial, M. J. Padgett, J. Cooper, and J. Laczik, Zsolt, "3D manipulation of particles into crystal structures using holographic optical tweezers," *Opt. Express* **12**, 220–226 (2004).
- [30] B. A. Koss and D. G. Grier, "Optical peristalsis," *Appl.*

- Phys. Lett. **82**, 3985–3987 (2003).
- [31] P. Reimann, “Brownian motors: Noisy transport far from equilibrium,” Phys. Rep. **361**, 57–265 (2002).
- [32] S.-H. Lee, K. Ladavac, M. Polin, and D. G. Grier, “Observation of flux reversal in a symmetric optical thermal ratchet,” Phys. Rev. Lett. **94**, 110601 (2005).
- [33] M. P. Hughes, “Strategies for dielectrophoretic separation in laboratory-on-a-chip systems,” Electrophoresis **23**, 2569–2582 (2002).
- [34] S.-H. Lee and D. G. Grier, “Flux reversal in a two-state symmetric optical thermal ratchet,” Phys. Rev. E, submitted for publication (2005).
- [35] L. Allen, M. W. Beijersbergen, R. J. C. Spreeuw, and J. P. Woerdman, “Orbital angular-momentum of light and the transformation of Laguerre-Gaussian laser modes,” Phys. Rev. A **45**, 8185–8189 (1992).
- [36] Z. S. Sacks, D. Rozas, and G. A. Swartzlander, “Holographic formation of optical-vortex filaments,” J. Opt. Soc. Am. B **15**, 2226–2234 (1998).
- [37] J. E. Curtis and D. G. Grier, “Structure of optical vortices,” Phys. Rev. Lett. **90**, 133901 (2003).
- [38] S. Sundbeck, I. Gruzberg, and D. G. Grier, “Structure and scaling of helical modes of light,” Opt. Lett. **30**, 477–479 (2005).
- [39] M. S. Soskin, V. N. Gorshkov, M. V. Vasnetsov, J. T. Malos, and N. R. Heckenberg, “Topological charge and angular momentum of light beams carrying optical vortices,” Phys. Rev. A **56**, 4064–4075 (1997).
- [40] H. He, M. E. J. Friese, N. R. Heckenberg, and H. Rubinsztein-Dunlop, “Direct observation of transfer of angular momentum to absorptive particles from a laser beam with a phase singularity,” Phys. Rev. Lett. **75**, 826–829 (1995).
- [41] H. He, N. R. Heckenberg, and H. Rubinsztein-Dunlop, “Optical particle trapping with higher-order doughnut beams produced using high efficiency computer generated holograms,” J. Mod. Opt. **42**, 217–223 (1995).
- [42] K. T. Gahagan and G. A. Swartzlander, “Optical vortex trapping of particles,” Opt. Lett. **21**, 827–829 (1996).
- [43] N. B. Simpson, L. Allen, and M. J. Padgett, “Optical tweezers and optical spanners with Laguerre-Gaussian modes,” J. Mod. Opt. **43**, 2485–2491 (1996).
- [44] A. T. O’Neil and M. J. Padgett, “Three-dimensional optical confinement of micron-sized metal particles and the decoupling of the spin and orbital angular momentum within an optical spanner,” Opt. Comm. **185**, 139–143 (2000).
- [45] A. T. O’Neil, I. MacVicar, L. Allen, and M. J. Padgett, “Intrinsic and extrinsic nature of the orbital angular momentum of a light beam,” Phys. Rev. Lett. **88**, 053601 (2002).
- [46] J. E. Curtis and D. G. Grier, “Modulated optical vortices,” Opt. Lett. **28**, 872–874 (2003).
- [47] K. Ladavac and D. G. Grier, “Microoptomechanical pump assembled and driven by holographic optical vortex arrays,” Opt. Express **12**, 1144–1149 (2004).
- [48] C.-S. Guo, X. Liu, J.-L. He, and H.-T. Wang, “Optimal annulus structures of optical vortices,” Opt. Express **12**, 4625–4634 (2004).
- [49] K. Ladavac and D. G. Grier, “Colloidal hydrodynamic coupling in concentric optical vortices,” Europhys. Lett. **70**, in press (2005).
- [50] A. Jesacher, S. Furrer, S. Bernet, and M. Ritsch-Marte, “Size selective trapping with optical ”cogwheel” tweezers,” Opt. Express **12**, 4129–4135 (2004).
- [51] J. Arlt, V. Garces-Chavez, W. Sibbett, and K. Dholakia, “Optical micromanipulation using a Bessel light beam,” Opt. Comm. **197**, 239–245 (2001).
- [52] V. Garces-Chavez, D. McGloin, H. Melville, W. Sibbett, and K. Dholakia, “Simultaneous micromanipulation in multiple planes using a self-reconstructing light beam,” Nature **419**, 145–147 (2002).
- [53] C. A. Alonzo, P. J. Rodrigo, and J. Glückstad, “Helico-conical optical beams: a product of helical and conical phase fronts,” Opt. Express **13**, 1749–1760 (2005).